

A Novel Absorption Resonance for Atomic Clocks

David F. Phillips*^{||}, Irina Novikova*, Sergei Zibrov*^{‡§}, Chris Smallwood[†]

Aleksei V. Taichenachev[¶], Valeriy I. Yudin[¶], Ronald L. Walsworth*[†], and Alexander S. Zibrov*^{‡§}

*Harvard-Smithsonian Center for Astrophysics, Cambridge MA 02138

[†]Department of Physics, Harvard University, Cambridge, Massachusetts, 02138

[‡]Moscow State Engineering Physics Institute, Moscow, 115409, Russia

[§]Lebedev Institute of Physics, Moscow, 117924, Russia

[¶]Institute of Laser Physics SB RAS and Novosibirsk State University, Novosibirsk, 630090, Russia

^{||}Email: dphil@cfa.harvard.edu

Abstract—We report an experimental study of an all-optical three-photon-absorption resonance (known as an “ N -resonance”) and discuss its potential application as an alternative to atomic clocks based on coherent population trapping (CPT). We present measurements of the N -resonance contrast, width and light shift for ^{87}Rb under various conditions including both D_1 and D_2 optical transitions. Under conditions such that first-order light shifts cancel, we observe promising short-term frequency stability ($\approx 1.5 \times 10^{-11} \tau^{-1/2}$) for an N -resonance on the D_1 transition of ^{87}Rb vapor.

I. INTRODUCTION

There is great current interest in developing small, economical atomic frequency standards with fractional frequency stability $\sim 10^{-12}$ or better. Significant progress toward this goal has been achieved using coherent population trapping (CPT) resonances in atomic vapor [1]. Recently our group demonstrated that a three-photon-absorption resonance (known as an “ N -resonance”) [2] is a promising alternative for small atomic clocks [3]. Here we report on the current status of investigations of N -resonance clocks, demonstrating high contrast resonances using both the D_1 and D_2 lines of rubidium, first-order cancellation of light shifts through optimization of intensity ratios of the optical fields, and preliminary clock stability measurements on a table-top apparatus.

N -resonances are a three-photon, two-field resonance (Fig. 1a). A probe field, Ω_P , resonant with the transition between the higher energy hyperfine level of the ground electronic state ($|b\rangle$) and an upper excited state ($|a\rangle$) optically pumps the atoms into the lower hyperfine state ($|c\rangle$), leading to increased transmission of the field through the medium. A second, off-resonant field, Ω_D is applied, detuned to lower frequencies than the $|b\rangle \rightarrow |a\rangle$ transition. If the difference frequency between Ω_P and Ω_D is equal to the hyperfine frequency, a two-photon resonance is created, driving atoms coherently from state $|c\rangle$ to $|b\rangle$ from which field Ω_P drives the atoms to the excited state leading to renewed absorption. Thus, on resonance, a reduction in the transmitted probe field is observed. The absorption spectrum of the Ω_P field has two features (Fig. 1a, bottom row): the broad Doppler background due to probe field linear absorption and the narrow resonance of the three-photon nonlinear process. Near 100% absorption of the probe field is observed on resonance, greatly

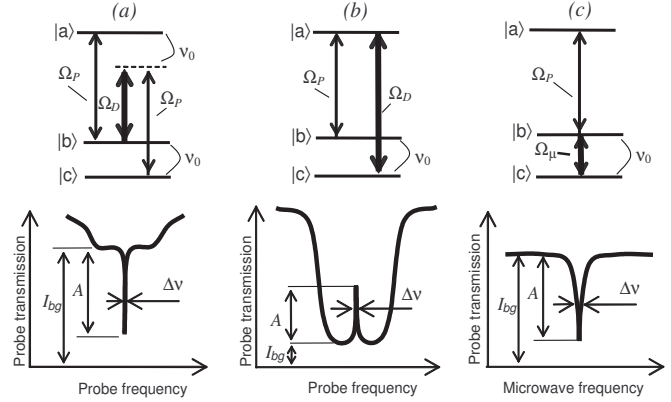


Fig. 1. Level diagrams (top row) and schematic representations of probe light transmission spectra for (a) N -resonance, (b) CPT resonance, and (c) optical-pumping double-resonance schemes. Shown in the level diagrams are the relevant probe (Ω_P), drive (Ω_D), and microwave fields (Ω_μ), as well as the ground-state hyperfine splitting ν_{hf} . Shown in the schematic spectra are the full width ($\Delta\nu$) and relative intensity (A) of the clock resonance, and the intensity of the background transmitted light (I_{bg}).

reducing the effects of shot noise as well as phase noise due to frequency/intensity conversion [4], [5].

For comparison, in figure 1 we also plot level diagrams and model resonances for CPT and traditional optically-pumped double-resonances. CPT is a transmission resonance (Fig. 1b) in which a coherence between two hyperfine levels is created by two resonant fields (Ω_P and Ω_D) whose frequency difference is equal to the hyperfine frequency. The absorption for both optical fields decreases due to destructive interference of the absorption probabilities, and a narrow transmission peak is observed. Several groups [5], [6] have achieved fractional stabilities below 10^{-12} with CPT-based clocks, which are also very promising for further miniaturization. In the traditional optically-pumped double-resonance clock (Fig. 1c), one optical field (from a lamp or laser diode) resonant with one of the allowed optical transitions ($|b\rangle \rightarrow |a\rangle$) pumps atoms to the other hyperfine sublevel ($|c\rangle$). When a microwave field is resonant with the groundstate hyperfine transition, it redistributes the populations between these two levels, leading to a narrow dip in the transmission spectrum. The width of this absorption feature is determined by the intensities of both

optical and microwave fields and the hyperfine decoherence rate. With careful optimization of various parameters short-term fractional stabilities of 10^{-11} may be achieved [7].

The frequency stability of an atomic clock limited only by shot noise is given by the Allan deviation, $\sigma(\tau)$, as [8]:

$$\sigma(\tau) = \frac{1}{4} \sqrt{\frac{\eta e}{I_{bg}} \frac{1}{\nu_{\text{hf}}} \frac{\Delta\nu}{C}} \tau^{-1/2} \quad (1)$$

where ν_{hf} is the atomic reference frequency, $\Delta\nu$ is the full width of the resonance, e is the electron charge, η is the photodetector sensitivity, and τ is the integration time. The contrast $C = A/I_{bg}$, where A is the resonance amplitude and I_{bg} is the intensity of the background transmitted light (adopting notation similar to [8]). These parameters for N -resonances, CPT resonances and optically pumped microwave double resonances, are shown in figure 1.

II. APPARATUS

Figure 2b shows a schematic of our experimental setup. We derived the two optical fields needed to probe the N -resonances by phase modulating the output of an external cavity diode laser [9] tuned in the vicinity of either the D_1 ($5^2S_{1/2} \rightarrow 5^2P_{1/2}$, $\lambda = 795$ nm) or the D_2 ($5^2S_{1/2} \rightarrow 5^2P_{3/2}$, $\lambda = 780$ nm) optical transition lines of Rb. An electro-optic modulator (EOM) [10] produced the phase modulation of the optical field at a frequency near the ground electronic state hyperfine frequency of ^{87}Rb ($\nu_{\text{hf}} \simeq 6.8$ GHz). We drove the EOM with a frequency synthesizer amplified to 1 to 5 watts. From 1.5% to 19% of the incident laser power was transferred to each first order sideband, depending upon the power applied to the EOM, with the remainder residing in the carrier. The laser beam was then circularly polarized using a quarter wave plate and weakly focused to a diameter of 0.8 mm before entering the Rb cell. The laser beam was then circularly polarized using a quarter wave plate and weakly focused to a diameter of 0.8 mm before entering the Rb cell.

We used various vapor cells filled with isotopically enriched ^{87}Rb and differing pressures of Ne, Ar, and N_2 with a total pressure between 25 and 100 Torr contained in Pyrex cylindrical cells (length 7 cm; diameter 2.5 cm). The vapor cells were heated to between 55 and 65 °C to provide an appropriate optical density of rubidium vapor. The cell was isolated from external magnetic fields with three layers of high permeability shielding. A small (≈ 10 mG) longitudinal magnetic field was applied to lift the degeneracy of the Zeeman sublevels and separate the $F = 1, m_F = 0$ to $F = 2, m_F = 0$ clock transition (with first order magnetic field independence) from the $m_F = \pm 1$ transitions which are sensitive to magnetic fields in first order and will thus suffer added broadening due to residual fluctuations in external fields.

To produce the N -resonance we tuned the high frequency sideband near resonance with the $5S_{1/2} F = 2, D_{1,2}$ transition. The strong laser carrier field at a frequency 6.8 GHz below this transition was used as the drive field Ω_D (Fig. 2a) while any effects from the weak and even-farther detuned lower frequency sideband were neglected. The probe field then carried the absorption signal of the N -resonance. Therefore, after passing through the vapor cell, the strong drive field and

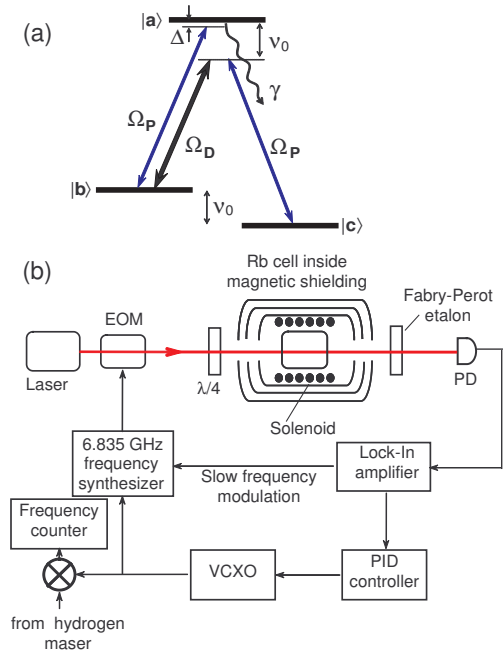


Fig. 2. (a) N -resonance interaction scheme. Ω_P and Ω_D are the probe and drive optical fields that create and interrogate the N -resonance, ν_{hf} is the hyperfine splitting of the two lower energy levels $|b\rangle$ and $|c\rangle$, γ is the collisionally-broadened decoherence rate of the excited state $|a\rangle$, and Δ is the one-photon detuning of the probe field from resonance with the $|b\rangle$ to $|a\rangle$ transition. (b) Schematic of the experimental setup. See text for abbreviations.

the off-resonant lower sideband were filtered from the laser beam using a quartz, narrow-band Fabry-Perot etalon (FSR=20 GHz, finesse=30), tuned to the frequency of the probe field.

For spectroscopic measurements, we phase-locked the 6.8 GHz synthesizer to a hydrogen maser and swept the synthesizer. We superimposed a slow frequency modulation at $f_m = 400$ Hz on the 6.8 GHz signal from the microwave synthesizer and demodulated the photodetector output at f_m with a lock-in amplifier. The system was run in open-loop with the output of the lock-in amplifier was monitored to record lineshapes, widths, and shifts. We also operated the N -resonance apparatus in a closed-loop mode in which the frequency of a VCXO (and hence the detuning of the probe and drive fields) was locked to the N -resonance, by using the lock-in output as an error signal to feed back to the VCXO (Fig. 2b). The microwave synthesizer was then locked to the output of the VCXO and we monitored the VCXO frequency (and thus the N -resonance center frequency) by comparing it to a signal derived from a hydrogen maser.

III. CONTRAST AND LINE WIDTH

N -resonance widths for two different cells are shown in Fig. 3. The width increases linearly with laser intensity with the narrowest observed resonance of ~ 300 Hz at 50 μW total laser power in the 40-Torr Ne cell. The linear dependence may be understood by analogy to optical pumping double resonance with an effective microwave field created by the combined action of the far-detuned drive and probe fields. The

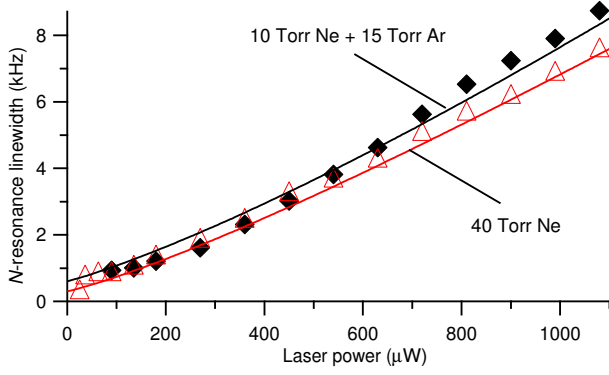


Fig. 3. Measured N -resonance linewidth, $\Delta\nu$, as a function of total incident laser power for ^{87}Rb vapor cells filled with 40-Torr of Ne buffer gas (\triangle) and a mixture of 10-Torr Ne and 15-Torr Ar (\blacklozenge). The probe field is tuned ≈ 300 MHz below the $F = 2 \rightarrow F' = 2$, D_1 transition of ^{87}Rb . The solid lines are calculated linewidths using an analytical N -resonance model.

corresponding Rabi frequency is $\Omega_\mu^{\text{eff}} = \Omega_P \Omega_D^* / \nu_{\text{hf}}$, where Ω_P and Ω_D are Rabi frequencies of the probe and drive fields. Applying the expression for the double-resonance width ($\Delta\nu$) from [7], we find

$$\Delta\nu = \left(\Gamma + \frac{\Omega_P^2}{2\gamma} \right) (S + 1)^{1/2} / \pi \quad (2)$$

where γ and Γ are the ground and excited state relaxation rates respectively, and S is power saturation factor of the microwave transition, $S = |\Omega_\mu^{\text{eff}}|^2 / (\Gamma + \Omega_P^2 / 2\gamma)^2$. Although (2) describes the qualitative dependence of the N -resonance width on laser power, direct substitution of the parameters above yield much broader widths than those observed. This is likely caused by the dual role played by the probe field as both the optical pumping field on the $|b\rangle \rightarrow |a\rangle$ transition and as an off-resonant Raman field on the $|c\rangle \rightarrow |a\rangle$ transition.

Measurements of the contrast $C = A/I_{bg}$ for two different cells are shown in Fig. 4. For both cells, the contrast increases rapidly and then saturates at $C \geq 15\%$ for total laser power ~ 1 mW due to optical pumping to other Zeeman levels. This saturated N -resonance contrast exceeds the contrast reported to date with traditional CPT clock resonances, $C < 4\%$ [8]. However, the relatively large laser power required to saturate the N -resonance contrast leads to an increased linewidth, $\Delta\nu$ (see Fig. 3), which reduces the frequency stability (see (1)).

To account for the trade-offs between contrast and linewidth, we follow [8], and define a resonance quality factor, q ,

$$q \equiv C / \Delta\nu \quad (3)$$

as a figure of merit for N -resonance clocks. For example, for 120 μW of laser power we find $\Delta\nu \approx 1$ kHz (Fig. 3, 40-Torr Ne cell) and $C \approx 0.1$ (Fig. 4), implying $q = 10^{-4} \text{ Hz}^{-1}$ and an estimated frequency stability (1) of $\sigma(\tau) \sim 10^{-14} \tau^{-1/2}$.

We also observe that the contrast of the N -resonance reaches its maximum at lower laser powers in the the 40-Torr Ne vapor cell than in the 25-Torr Ne-Ar mixture. We attribute this difference to slower Rb diffusion out of the laser fields

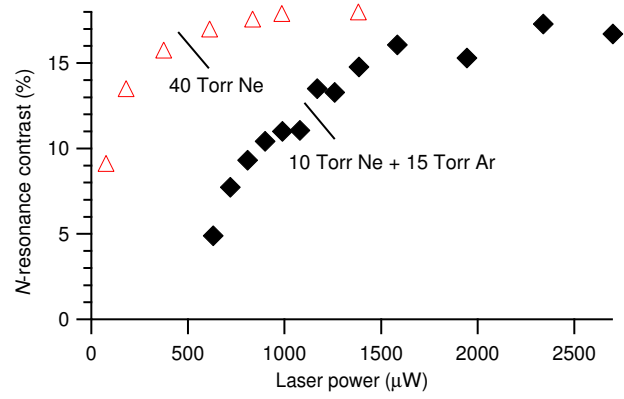


Fig. 4. Measured N -resonance contrast, C , as a function of total incident laser power for ^{87}Rb vapor cells filled with 40-Torr of Ne buffer gas (\triangle) and a mixture of 10-Torr Ne and 15-Torr Ar (\blacklozenge). The probe field is tuned ≈ 300 MHz below the $F = 2 \rightarrow F' = 2$, D_1 transition of ^{87}Rb . The solid lines are calculated linewidths using an analytical N -resonance model.

at higher buffer gas pressure, and hence reduced ground-state coherence loss and more efficient optical pumping. In addition, we did not detect any deterioration of the N -resonance contrast with increasing buffer gas pressure as has been observed in CPT resonances [8]. This suggests that the N -resonance may be a good candidate for miniature atomic clocks where high buffer gas pressure is required to prevent rapid decoherence due to collisions with the walls of a small vapor cell.

IV. COMPARISON OF D_1 AND D_2 TRANSITIONS

Comparing the results above for N -resonances with published data for CPT clocks, we find much higher contrasts for N -resonances. Despite the increased N -resonance width due to power broadening, the quality figure q (see (3)) for N -resonances is comparable with the best existing results for CPT clocks [8]. However, many CPT contrast measurements to date have been performed on the D_2 optical transition while the data presented above is for D_1 . The D_1 line may improve both resonance contrast and width of existing CPT clocks [11]. Therefore, in this section, we compare measured N -resonance widths and contrasts for the D_2 and D_1 optical transitions.

In a warm vapor cell, a pure dark state exists only for the D_1 transition. The ratio of transition strengths from the ground states to an excited electronic state hyperfine level of the D_1 transition is the same for both excited-state hyperfine levels [12]. Thus a ground-state superposition that is dark to one excited-state hyperfine level is also a dark state for the other level (Fig. 5a). For the D_2 transition (Fig. 5b), the ratio of transition strengths differ for each excited state [12], and thus, an atom in a dark state for light resonant with one excited state will not be in a dark state for other excited state levels. Velocity-changing collisions in the warm vapor cell will shift the one-photon detuning such that atoms will couple to all excited-state hyperfine levels, destroying the dark state in the D_2 transition.

CPT resonances, whose atomic state is a “dark state” super-

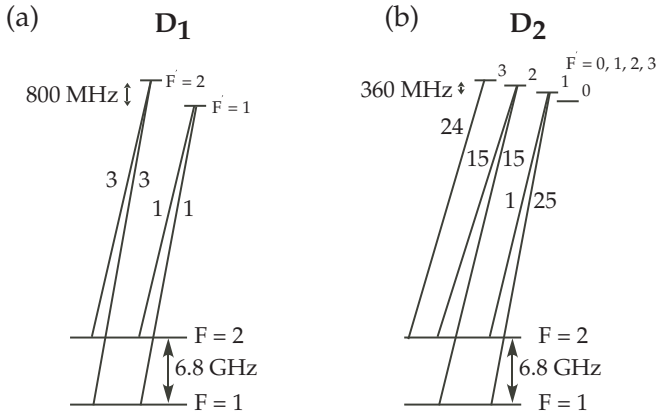


Fig. 5. Relative transition strengths for $F = 1, 2; m = 0 \rightarrow F'$; $m = 1$ transitions in (a) the D_1 optical transition and (b) the D_2 transition of ^{87}Rb [12]. Energy spacings are not shown to scale. Note that in (a), a dark state of the $F' = 1$ optical transition is also a dark state of the $F' = 2$ transition because the ratio of transition elements are equal. In (b), there is no dark state that is independent of the excited state hyperfine level addressed.

position between the $F = 1, m_F = 0$ and $F = 2, m_F = 0$ states, therefore have much higher amplitude for the D_1 line than D_2 [11]. For N -resonances, the two-photon absorption resonance does not require a dark state. Therefore, we expect no noticeable advantages for D_1 line excitation over the D_2 .

Additionally, for circularly polarized light (which is usually used in optically-pumped atomic clocks) resonant with the D_1 transition, many atoms are trapped in the Zeeman state with maximum angular momentum - an “end” state ($F = 2, m_F = \pm 2$ for ^{87}Rb) [13]. This limits the resonance amplitude and contrast of both N -resonances and CPT resonances from the $m_F = 0$ clock transition. However, for the D_2 line the end Zeeman state is coupled to the excited state through the cycling transition $F = 2 \rightarrow F' = 3$. In the presence of strong collisional mixing in the excited state, the cycling transition suppresses optical pumping of atoms into the end state. Thus we expect higher resonance contrast for N -resonances on the D_2 transition.

In the data presented in this section, a vapor cell containing 100-Torr Ne buffer gas ($\gamma/\pi \approx 2$ GHz) was heated to 65°C . For both the D_1 and D_2 transitions, the modulation index was 0.38, corresponding to a probe/drive field intensity ratio of 19%. Sample N -resonances for the D_1 and the D_2 lines under similar conditions are shown in Fig. 6. The amplitude of the D_2 N -resonance ($\approx 30\%$) is significantly larger than that for the D_1 line ($\approx 12\%$), while its width is slightly broader (4.4 kHz for the D_2 vs. 3.0 kHz for the D_1 line). The quality factor, q , defined in (3) is only slightly degraded in the D_2 transition compared to D_1 , because the larger D_2 linewidth is compensated by a higher contrast. Note, that this situation is different from CPT resonances [11], [14] where the quality figure for the D_2 line is almost an order of magnitude worse than that for the D_1 line.

As phase sensitive detection is commonly used in optically-pumped frequency standards to produce a lock-loop feedback

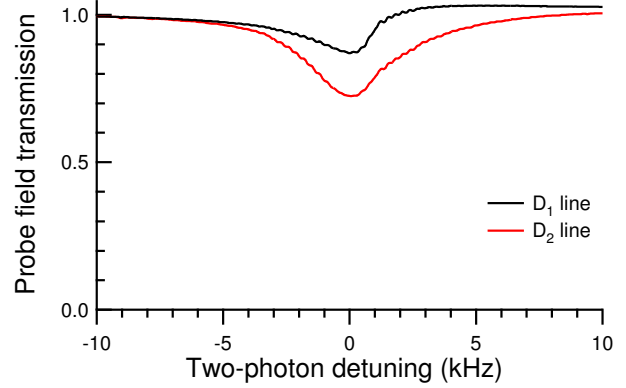


Fig. 6. Sample N -resonance observed for the D_1 and the D_2 optical transitions. Laser power of $260 \mu\text{W}$, corresponding to an intensity of $\approx 50 \text{ mW/cm}^2$. Probe field transmission is normalized to unity away from two-photon resonance.

signal, an asymmetric resonance lineshape leads to additional frequency shifts proportional to modulation parameters [15]. As shown in Fig. 6, we observe more symmetric resonances from the N -resonance on the D_2 line than the D_1 line, giving an additional advantage for the use of the D_2 line in N -resonance clocks.

V. LIGHT SHIFTS

The stability of optically-pumped atomic clocks is often limited by the “light shift,” an AC Stark effect that shifts the atomic levels [16] depending on both the optical field frequency and intensity. Fluctuations in these parameters are directly transferred to the clock frequency. Light shifts remain the limiting factor for the stability of optically pumped double resonance clocks at the level of 10^{-11} [17]–[19].

In CPT clocks, in principle, the light shift may be almost completely eliminated. Typically, however, the diode laser is driven with current-modulation to produce the two strong, resonant optical fields. This necessarily leads to higher order sidebands, which, even when optimally adjusted, can lead to second order light shifts [20]. Amplitude modulation (AM) is also usually present when current modulation is used to create resonant sidebands. The resulting imbalance in sideband intensities is often as large as 10% for CPT clocks [5]. This imbalance leads to linear light shifts observed to be of order 0.1 to 0.3 Hz/ $\mu\text{W/cm}^2$ and 1 Hz/MHz [5], [6], [8].

For the idealized three-level N -resonance of Fig. 2a, the light shift δ_{ls} (i.e., the detuning from ν_{hf} of the difference frequency between the probe and drive fields, as measured by maximum probe field absorption) consists of three leading (first-order) terms: shifts of both ground-states due to interaction with the strong, far-detuned drive field, and a shift of ground-state $|c\rangle$ due to interaction with the near-resonant probe field:

$$\delta_{\text{ls}} \approx -\frac{|\Omega_D|^2}{\nu_{\text{hf}} + \Delta} + \frac{|\Omega_D|^2}{2\nu_{\text{hf}} + \Delta} + \frac{|\Omega_P|^2 \Delta}{\Delta^2 + \gamma^2/4}. \quad (4)$$

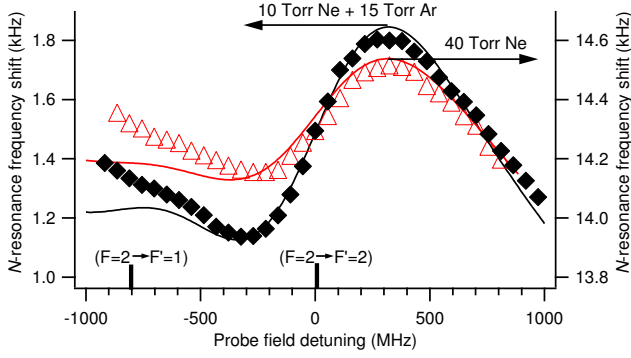


Fig. 7. Measured variation of the N -resonance frequency as a function of probe field detuning from the ^{87}Rb $F = 2 \rightarrow F' = 2$ transition with total incident laser power of $450 \mu\text{W}$. Right vertical axis: 40-Torr Ne (Δ). Left vertical axis: 25-Torr Ne-Ar mixture (\blacklozenge). These N -resonance frequencies include a buffer gas pressure shift of the ^{87}Rb ground-state hyperfine frequency: 14 kHz for the 40-Torr Ne cell and 1 kHz for the 25-Torr Ne-Ar mixture [21], [22]. The solid lines are calculations from an analytical model.

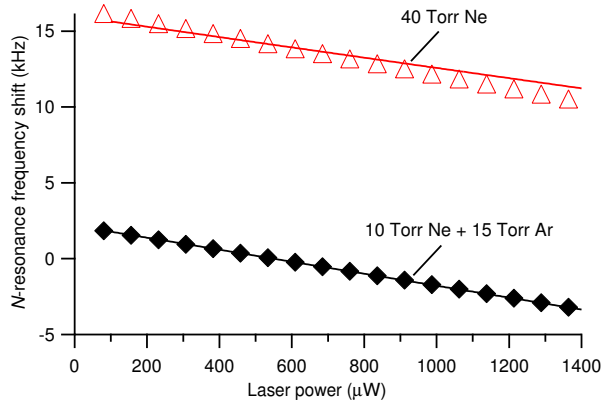


Fig. 8. The dependence of the N -resonance frequency on the total laser power in the cells with the 25-Torr Ne-Ar mixture (\blacklozenge) and with 40-Torr of Ne (Δ). The probe field is tuned to the $F = 2 \rightarrow F' = 1$ transition of ^{87}Rb .

Here Δ is the one-photon detuning of the probe field from resonance, γ is the collisionally-broadened decoherence rate of the excited state, and Ω_P and Ω_D are the probe and drive fields' Rabi frequencies. The light shifts due to the far-detuned drive field (the first and second terms in (4)) are proportional to the drive field intensity, but practically independent of the laser frequency for $\Delta \ll \nu_{\text{hf}}$. In contrast, the light shift due to the near-resonant probe field (the last term in (4)) has a strong dispersive-like dependence on Δ . Thus, near the extrema, $\Delta = \pm\gamma/2$, the total N -resonance light shift has only a quadratic dependence on the probe field detuning (see Fig. 7):

$$\delta_{\text{ls}} \approx -\frac{|\Omega_D|^2}{2\nu_{\text{hf}}} \pm \frac{|\Omega_P|^2}{\gamma} \mp \frac{2|\Omega_P|^2}{\gamma^3} (\Delta \mp \gamma/2)^2. \quad (5)$$

This light shift can then be canceled by (i) detuning the probe field to the high-frequency extremum, and (ii) properly setting

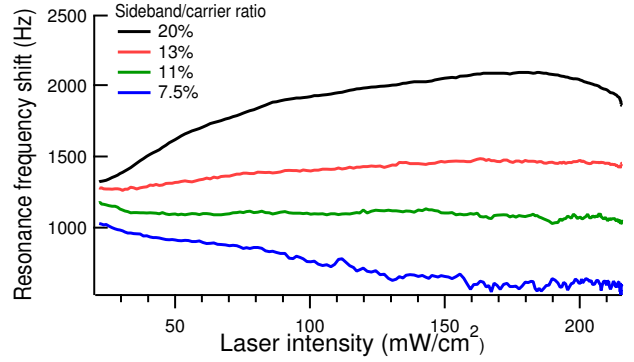
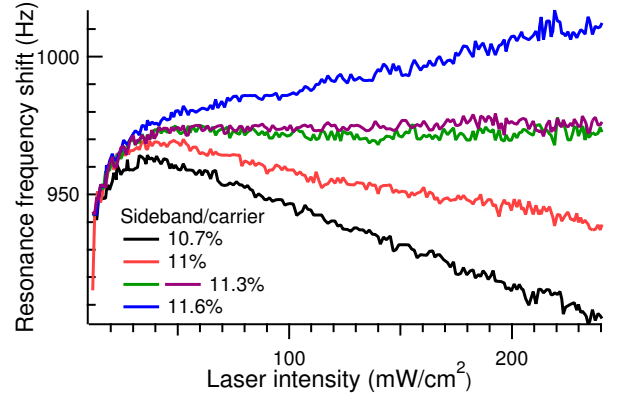


Fig. 9. Measured intensity light-shift: N -resonance frequency shift as a function of laser intensity for different ratios between the probe and drive field intensities (e.g., ratios of sideband/carrier intensities) with probe field detuned to the light-shift maximum ($\Delta \approx 700 \text{ MHz}$). (a) D_1 optical transition in a 15-Torr Ne, 15-Torr Ar, and 5-Torr N_2 ^{87}Rb vapor cell; and (b) D_2 optical transition in a 100-Torr Ne ^{87}Rb vapor cell.

the intensity ratio of the drive and probe fields:

$$\Delta = +\gamma/2, \quad \frac{|\Omega_P|^2}{|\Omega_D|^2} = \frac{\gamma}{2\nu_{\text{hf}}}. \quad (6)$$

With such light-shift cancellation, the measured N -resonance center frequency should be insensitive (to leading order) to fluctuations of the probe field frequency and total laser intensity. Note that the light-shift cancellation does not depend on the absolute intensity of the optical fields.

To verify these predictions, we measured ^{87}Rb N -resonance light shifts using the experimental setup shown in Fig. 2b and described above with vapor cells containing several mixtures and pressures of buffer gases. N -resonance light shifts are shown in figures 7 and 8 for 25-Torr Ne-Ar mixture and 40-Torr Ne vapor cells. As the probe field frequency is varied through the D_1 , $F = 2 \rightarrow F' = 1, 2$ transition (Fig. 7), two extrema are observed demonstrating the quadratic light-shift dependence on laser detuning of (5). Additionally, the curvature is reduced in the higher buffer gas pressure vapor cell from approximately 4.0 mHz/MHz^2 for the 25-Torr Ne-Ar mixture to 2.5 mHz/MHz^2 for the 40-Torr Ne, suggesting that the N -resonance may be well suited to high buffer gas pressure, small vapor cells. The dependence of the light shift

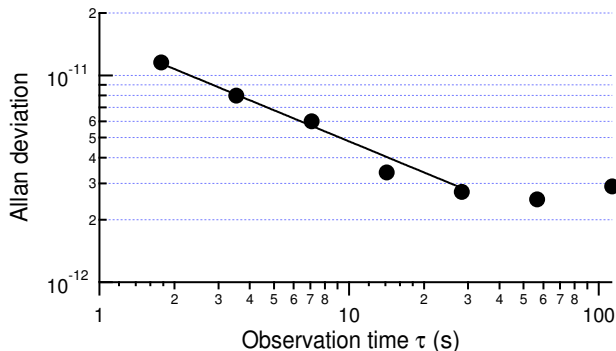


Fig. 10. Measured fractional frequency stability, $\delta\nu/\nu$, of a 100 MHz crystal oscillator locked to the ^{87}Rb N -resonance, relative to a hydrogen maser.

in the N -resonance measured for different laser intensities is shown in Fig. 8. In this case the shift is linear in total laser intensity, and again the slope of this line decreases as the buffer gas pressure in the cell increases (20 mHz/($\mu\text{W}/\text{cm}^2$) for 40-Torr of Ne versus 27 mHz/($\mu\text{W}/\text{cm}^2$) for the 25-Torr Ne-Ar mixture).

In additional measurements, we study the light-shift compensation point using a ^{87}Rb vapor cell with a buffer gas mixture of 15-Torr Ne, 15-Torr Ar, and 5-Torr N_2 (chosen to minimize the temperature dependence of the ^{87}Rb ground-state hyperfine frequency shift due to buffer gas collisions [7]; pressure broadened excited state linewidth $\gamma/\pi \approx 1.2$ GHz), as well as with a 100-Torr Ne vapor cell. Figure 9 shows examples of the measured dependence of the N -resonance frequency on laser intensity and probe/drive intensity ratio for both D_1 and D_2 optical transitions. The intensity light-shift cancellation ratio, $|\Omega_P|^2/|\Omega_D|^2 \approx 11\%$, is in reasonable agreement with the prediction of $|\Omega_P|^2/|\Omega_D|^2 \approx 9\%$ given by (6) for our experimental conditions.

VI. FREQUENCY STABILITY

Finally, we characterized the frequency stability of a crude “ N -resonance clock” — i.e., the VCXO locked to the ^{87}Rb N -resonance as described above — relative to a hydrogen maser. For this measurement we used a 15-Torr Ne, 15-Torr Ar, and 5-Torr N_2 buffer gas vapor cell and tuned our system to the conditions for optimal light-shift cancellation (laser detuning $\Delta \approx 700$ MHz, probe/drive intensity ratio $\approx 11\%$) with total laser power $\approx 140 \mu\text{W}$ (intensity $\approx 30 \text{ mW}/\text{cm}^2$). Under such conditions the N -resonance linewidth ≈ 1400 Hz (FWHM) and contrast $\approx 7\%$, which implies a shot-noise-limited short-term frequency $\approx 5 \times 10^{-14} \tau^{-1/2}$ [8]. Figure 10 shows the measured N -resonance clock fractional frequency stability (Allan deviation). The short-term stability $\approx 1.5 \times 10^{-11} \tau^{-1/2}$ for observation times $1 \text{ s} \lesssim \tau \lesssim 50 \text{ s}$. At longer times the stability degrades due to uncontrolled temperature and mechanical variations in our table-top apparatus, as well as long-term drifts of the laser frequency. Despite this non-optimal clock apparatus, the short-term N -resonance frequency stability is already better than that provided by many recently-

demonstrated CPT clocks [1], [6], [23]. We expect that both the short- and long-term N -resonance frequency stability can be further improved by straightforward optimization of the VCXO lock-loop (to reduce phase noise), temperature stabilization, laser control, etc. We also expect that a high-stability N -resonance clock should be possible in a compact physical package (with vapor cell volume $\sim 1 \text{ mm}^3$), because of promising N -resonance characteristics at high buffer gas pressure.

VII. CONCLUSIONS

In conclusion, we have presented a summary of the current status of an all-optical, three-photon-absorption N -resonance clock. We have characterized the contrast and linewidth of such resonances on both the D_1 and D_2 optical transitions of ^{87}Rb and find the overall quality competitive with CPT resonances. We found that the lineshape for the D_2 is more symmetric than the D_1 line, making it perhaps less sensitive to slow-modulation induced effects. Thus, both optical transitions may work well for N -resonance clocks as opposed to CPT resonances in which performance is compromised by the use of the optical D_2 transition.

We also demonstrated cancellation of first-order light-shifts on the D_1 line of ^{87}Rb vapor. Employing this light-shift cancellation in a table-top apparatus, we observed N -resonance frequency stability comparable to or better than existing CPT clocks. Significant improvements in N -resonance frequency stability should be possible in a small device with standard techniques.

REFERENCES

- [1] J. Vanier, “Atomic clocks based on coherent population trapping: a review,” *Appl. Phys. B*, vol. 81, pp. 421–442, 2005.
- [2] A. S. Zibrov, C. Y. Ye, Y. V. Rostovtsev, A. B. Matsko, and M. O. Scully, “Observation of a three-photon electromagnetically induced transparency in hot atomic vapor,” *Phys. Rev. A*, vol. 65, p. 043817, 2002.
- [3] S. Zibrov, I. Novikova, D. F. Phillips, A. V. Taichenachev, V. I. Yudin, R. L. Walsworth, and A. S. Zibrov, “Three-photon-absorption resonance for all-optical atomic clocks,” *Phys. Rev. A*, vol. 72, p. 011801(R), 2005.
- [4] J. C. Camparo and W. F. Buell, “Laser PM to AM conversion in atomic vapors and short term clock stability,” in *Proc. IEEE Intl. Freq. Cont. Symp.*, IEEE, New York, 1997, pp. 253–258.
- [5] S. Knappe, R. Wynands, J. Kitching, H. G. Robinson, and L. Hollberg, “Characterization of coherent population-trapping resonances as atomic frequency references,” *J. Opt. Soc. Am. B*, vol. 18, p. 1545, 2001.
- [6] M. Merimaa, T. Lindwall, I. Tittonen, and E. Ikonen, “All-optical atomic clock based on coherent population trapping in ^{85}Rb ,” *J. Opt. Soc. Am. B*, vol. 20, p. 273, 2003.
- [7] J. Vanier and C. Audoin, *The Quantum Physics of Atomic Frequency Standards*. New York: Hilger, 1989.
- [8] J. Vanier, M. W. Levine, D. Janssen, and M. J. Delaney, “On the use of intensity optical pumping and coherent population trapping techniques in the implementation of atomic frequency standards,” *IEEE T. Instrum. Meas.*, vol. 52, pp. 822–831, 2003.
- [9] New Focus Vortex laser model 6017.
- [10] New Focus phase modulator model 4851.
- [11] M. Stahler, R. Wynands, S. Knappe, J. Kitching, L. Hollberg, A. Taichenachev, and V. Yudin, “Coherent population trapping resonances in thermal Rb-85 vapor: D-1 versus D-2 line excitation,” *Opt. Lett.*, vol. 27, p. 1472, 2002.
- [12] H. J. Metcalf and P. van der Straten, *Laser Cooling and Trapping*. New York: Springer, 1999.

- [13] Y.-Y. Jau, A. B. Post, N. N. Kuzma, A. M. Braun, M. V. Romalis, and W. Happer, "Intense, narrow atomic-clock resonances," *Phys. Rev. Lett.*, vol. 92, p. 110801, 2004.
- [14] R. Lutwak, D. Emmons, T. English, W. Riley, A. Duwel, M. Varghese, D. K. Serkland, and G. M. Peake, "testing," in *Proceedings of the 35th Annual Precise Time and Time Interval (PTTI) Systems and Applications Meeting*, U.S. Naval Observatory, Washington, D.C., 2003, p. 467.
- [15] D. F. Phillips, I. Novikova, C. Y.-T. Wang, M. Crescimanno, and R. L. Walsworth, "Modulation-induced frequency shifts in a coherent-population-trapping-based atomic clock," *J. Opt. Soc. Am. B*, vol. 22, p. 305, 2005.
- [16] B. S. Mathur, H. Tang, and W. Happer, "Light shifts in alkali atoms," *Phys. Rev.*, vol. 171, p. 11, 1968.
- [17] L. A. Budkin, V. L. Velichanskii, A. S. Zibrov, A. A. Lyalyaskin, M. N. Penenkirov, and A. I. Pikhitev, "Double radio-optical resonance in alkali metal vapors subjected to laser excitation," *Sov. J. Quant. Electron.*, vol. 20, p. 301, 1990.
- [18] J. C. Camparo and S. B. Delcamp, "Optical pumping with laser-induced-fluorescence," *Opt. Commun.*, vol. 120, p. 257, 1995.
- [19] G. Miletì, J. Deng, F. L. Walls, D. A. Jennings, and R. E. Drullinger, "Laser-pumped rubidium frequency standards: New analysis and progress," *IEEE J. Quantum Electron.*, vol. 34, p. 233, 1998.
- [20] J. Vanier, A. Godone, and F. Levi, "Coherent population trapping in cesium: Dark lines and coherent microwave emission," *Phys. Rev. A*, vol. 58, p. 2345, 1998.
- [21] C. Ottinger, R. Scheps, G. W. York, and A. Gallagher, "Broadening of the rb resonance lines by the noble gases," *Phys. Rev. A*, vol. 11, p. 1815, 1975.
- [22] M. Erhard and H. Helm, "Buffer-gas effects on dark resonances: theory and experiment," *Phys. Rev. A*, vol. 63, p. 043813, 2001.
- [23] S. Knappe, P. D. D. Schwindt, V. Shah, L. Hollberg, J. Kitching, L. Liew, and J. Moreland, "A chip-scale atomic clock based on ^{87}Rb with improved frequency stability," *Opt. Express*, vol. 13, p. 1249, 2005.